Epithelial cell transforming factor ECT2 is an important regulator of DNA double-strand break repair and genome stability

Cheng Cao[1], Peiyi Han[1], Ling Liu[1], Yiman Tang[2], Shanshan Tian[1], Kai Zhang[1], Lei Shi[1], Zhiqiang Liu[1], Dexiang Zhuo[3,*], Wenshu Ge[2,*], and Wenchen Gong[1,*]

From the [1]Tianjin Medical University Cancer Institute and Hospital, The Province and Ministry Co-Sponsored Collaborative Innovation Center for Medical Epigenetics, Key Laboratory of Immune Microenvironment and Disease (Ministry of Education), Key Laboratory of Breast Cancer Prevention and Therapy (Ministry of Education), School of Basic Medical Sciences, Tianjin Medical University, Tianjin, China; [2]Department of General Dentistry II, Peking University School and Hospital of Stomatology, Beijing, China; [3]Department of Laboratory Medicine, The Central Laboratory of the Sanming First Hospital Affiliated to Fujian Medical University, Sanming, China

Edited by Patrick Sung

Proteins containing breast cancer type 1 (BRCA1) C-terminal domains play crucial roles in response to and repair of DNA damage. Epithelial cell transforming factor (epithelial cell transforming sequence 2 [ECT2]) is a member of the BRCA1 C-terminal protein family, but it is not known if ECT2 directly contributes to DNA repair. In this study, we report that ECT2 is recruited to DNA lesions in a poly (ADP-ribose) polymerase 1–dependent manner. Using co-immunoprecipitation analysis, we showed that ECT2 physically associates with KU70–KU80 and BRCA1, proteins involved in nonhomologous end joining and homologous recombination, respectively. ECT2 deficiency impairs the recruitment of KU70 and BRCA1 to DNA damage sites, resulting in defective DNA double-strand break repair, an accumulation of damaged DNA, and hypersensitivity of cells to genotoxic insults. Interestingly, we demonstrated that ECT2 promotes DNA repair and genome integrity largely independently of its canonical guanine nucleotide exchange activity. Together, these results suggest that ECT2 is directly involved in DNA double-strand break repair and is an important genome caretaker.

Cells need efficient DNA repair tools to respond to DNA damage so that genetic information can be transmitted and cellular phenotype can be maintained (1, 2). DNA double-strand breaks (DSBs) are one of the most deleterious types of DNA damage because misrepair of DSB can cause severe point mutations, deletions, and chromosome rearrangements (3, 4). The two major pathways that contribute to DSB repair are nonhomologous end joining (NHEJ) and homologous recombination (HR) (5–7). Generally, double-stranded DNA ends are rapidly and efficiently bound by the KU70-KU80 heterodimer because of their high abundance and an intrinsically avid end-binding capacity (8). The KU–DNA complex further recruits the catalytic subunit of DNA–protein kinase (DNA-PKcs), DNA ligase IV,

X-ray cross-complementing group 4, and X-ray cross-complementing group 4–like factor to promote NHEJ (7). In a resection-competent state, KU dimers are removed by the C-terminal-binding protein interacting protein/MRE11-RAD50-NBS1 (MRN) complex-directed limiting 5′ to 3′ end resection. Then, the exonucleases DNA2 and EXO1 extend the length of the resected DNA, and DNA repair occurs via the HR pathway (7, 9).

Once DSBs occur, the DNA damage response (DDR) machinery detects DNA damage and transduces a cellular signaling response, and the DSBs are repaired in an organized manner, for example, by NHEJ or HR, to protect the genome (4, 10, 11). DDR factors are spatiotemporally concentrated at sites of DNA damage on damaged chromatin (11), where they can be visualized by microscopy as discrete nuclear foci or micro-irradiation (IR) path. The assembly and transduction of DDR cascades rely on a broad spectrum of post-translational modifications, including phosphorylation, which is involved in the recruitment and release of DDR factors (3, 11–15). Proteins that are phosphorylated in response to DNA damage are recognized by breast cancer type 1 (BRCA1) C-terminal (BRCT) domain–containing proteins, which can either transmit signals to DNA repair machinery or target diverse proteins into repair complexes (16–18). For example, mediator of DNA damage checkpoint 1 (MDC1) directly binds phospho-Ser139 on H2AX (γH2AX) through its C-terminal BRCT repeats (19, 20). In addition, the breast cancer tumor-suppressor protein BRCA1 recognizes phosphoserine-containing peptides derived from the DNA repair helicase BACH1 and the end resection–associated protein C-terminal-binding protein interacting protein (21–23).

Epithelial cell transforming sequence 2 (ECT2; also known as ARHGEF31) has two tandem BRCT domains in the N terminus and contains Dbl homology (DH) catalytic and pleckstrin homology (PH) regulatory domains in the C terminus (24–26). ECT2 is a member of the Ras homologous (Rho) family of guanine nucleotide exchange factors (GEFs) and so primarily activates small GTPases including Ras

* For correspondence: Wenchen Gong, gongwenchen@tmu.edu.cn; Wenshu Ge, esther1234@hsc.pku.edu.cn; Dexiang Zhuo, wubishou@fjmu.edu.cn.

homolog family member A (RhoA), Rac family small GTPase 1 (RAC1), and cell division cycle 42 (CDC42) (24, 27, 28). It is well documented that ECT2 regulates cytokinesis in non-transformed cells by targeting RhoA (29) and that ECT2 drives transformation by activating RAC1 (30, 31). During the interphase of the cell cycle, the ECT2–CDC42 pathway controls the incorporation of histone variant CENP-A at centromeres (32), and ECT2–RAC1 promotes ribosomal DNA transcription (33). Although ECT2 is localized at DNA damage sites (34), it is not known if ECT2 is involved in DSB repair or how it contributes to DDR. Recently, we discovered that ECT2 promotes dimerization and stabilization of the ubiquitin-specific protease USP7 independently of its nuclear GEF activity (35). This finding prompted us to investigate the role of ECT2 in DSB repair, and whether the repair mechanisms are mediated by the GEF activity of ECT2.

We found that ECT2 is localized to damaged chromatin and localization is driven by the catalytic activity of poly(ADP-ribose) polymerase 1 (PARP1). We also showed that ECT2 promotes HR and NHEJ repair of DSBs, independently of GEF activity, by facilitating the assembly of BRCA1 and KU complexes on damaged chromatin.

Results

ECT2 is recruited to DNA damage sites

To investigate whether ECT2 is involved in the response to and repair of DNA DSBs, we first examined the recruitment of ECT2 at DSBs induced by the endonuclease AsiSI in HeLa cells stably expressing the estrogen receptor (ER) fused to AsiSI (ER-AsiSI) (36, 37). In this system, DSBs are generated by nuclear-localized ER-AsiSI when cells are treated with 4-hydroxytamoxifen (4-OHT) (Fig. S1A). Concomitant with the incorporation of γH2AX, chromatin immunoprecipitation (ChIP) analysis showed that after 4-OHT induction, ECT2 was detected at the DSB proximal site approximately 3.7 kb from the break site, but not the distal region about 2 Mb from the break site (Fig. 1A). The expression level of ECT2 did not alter following the induction of DSBs (Fig. 1B).

Fractionation of the cellular extracts from ER-AsiSI HeLa cells followed by immunoblotting demonstrated that after DSB, nuclear ECT2 preferentially accumulated in the chromatin fraction and decreased in the soluble fraction (Fig. 1C). Furthermore, immunofluorescence staining followed by confocal microscopy analysis indicated that endogenous ECT2 accumulated at UVA laser microdissection–induced DNA lesions marked by γH2AX expression (Fig. 1D). The specificity of results obtained using an ECT2 antibody was confirmed by siRNA-mediated knockdown (Fig. S1B). These results suggest that DNA damage causes ECT2 to be mobilized and recruited to DSB sites.

PARP1 controls the recruitment of ECT2

To understand how the recruitment of ECT2 is regulated, U2OS cells were treated with inhibitors of ataxia–telangiectasia mutated, DNA-PKcs, and PARP1. UVA laser microdissection followed by confocal microscopy analysis showed that olaparib (a PARP1 inhibitor) significantly impaired ECT2 recruitment, but KU55933 (an ataxia telangiectasia mutated inhibitor) and NU7026 (a DNA-PKcs inhibitor) did not affect ECT2 relocalization (Fig. 2A). PARP1 depletion by two distinct siRNAs also weakened the formation of ECT2 laser stripes on damaged chromatin (Fig. 2B). Immunoblotting confirmed that the siRNAs reduced the expression of PARP1 (Fig. 2B). Meanwhile, chromatin fractionation analysis of ER-AsiSI cells demonstrated that olaparib treatment reduced the recruitment of ECT2 to damaged chromatin (Fig. S2A). These results suggest that the catalytic activity of PARP1 localizes ECT2 to DNA damage sites.

Because ECT2 can recognize poly(ADP-ribosyl)ation (PARylation) of α-tubulin through its BRCT domains (38), we wondered whether this mechanism is conserved in DDR. To test this hypothesis, we replaced lysine 195 (K195) with alanine to generate an ECT2/K195A mutant that could not bind PAR *in vitro* and could not bind PARylated α-tubulin *in vivo* (38). We used laser micro-IR and live-cell imaging to examine the formation of laser stripes in cells expressing ECT2/K195A. K195A point mutation within the full length of ECT2 mildly reduced its recruitment to DNA lesions (Fig. 2C). When the K195A mutation was restricted to the N-terminal BRCT domain (N-K195A), ECT2 almost completely failed to localize at damage sites (Fig. 2C). These results implied that regions other than BRCTs may also contribute to the accumulation of ECT2 at DNA lesions. Interestingly, we showed that the C-terminal region containing DH and PH domains also formed laser stripes upon micro-IR (Fig. 2D), and the recruitment of either N-terminal-truncated or C-terminal-truncated ECT2 was sensitive to olaparib treatment (Fig. 2D). Next, we found knockdown of ECT2 expression did not affect the level of poly-ADP ribose (PAR) moieties of total proteins upon DNA damage, suggesting that ECT2 acts downstream of PARP1-catalyzed PARylation, and that it is unlikely that ECT2 is involved in PAR synthesis and degradation (Fig. S2, B and C). These results suggest that the enrichment of ECT2 at DNA damage sites relies on the catalytic activity of PARP1 and that several distinct regions of ECT2 are involved in this process.

ECT2 is required for efficient HR and NHEJ

To address the functional significance of ECT2 recruitment at DSB sites, we examined the role of ECT2 in NHEJ and HR. To monitor NHEJ efficiency, a DNA fragment with two recognition sites for the I-SceI endonuclease followed by a GFP gene coding fragment was stably integrated into U2OS cells (Fig. 3A). The cutting and removal of the two I-SceI sites by I-SceI triggered NHEJ to eliminate the otherwise nonsense transcript and enable GFP expression; the percentage of cells expressing GFP protein reflects the efficiency of NHEJ repair. Using this reporter system, we found that knockdown of ECT2 expression reduced the percentage of GFP-positive cells (Fig. 3A), suggesting that ECT2 is required for efficient NHEJ. Immunoblotting confirmed that ECT2 expression was knocked down after siRNA treatment (Fig. 3A).

Next, we monitored the efficiency of HR repair using a DR-GFP reporter system in which a construct containing two
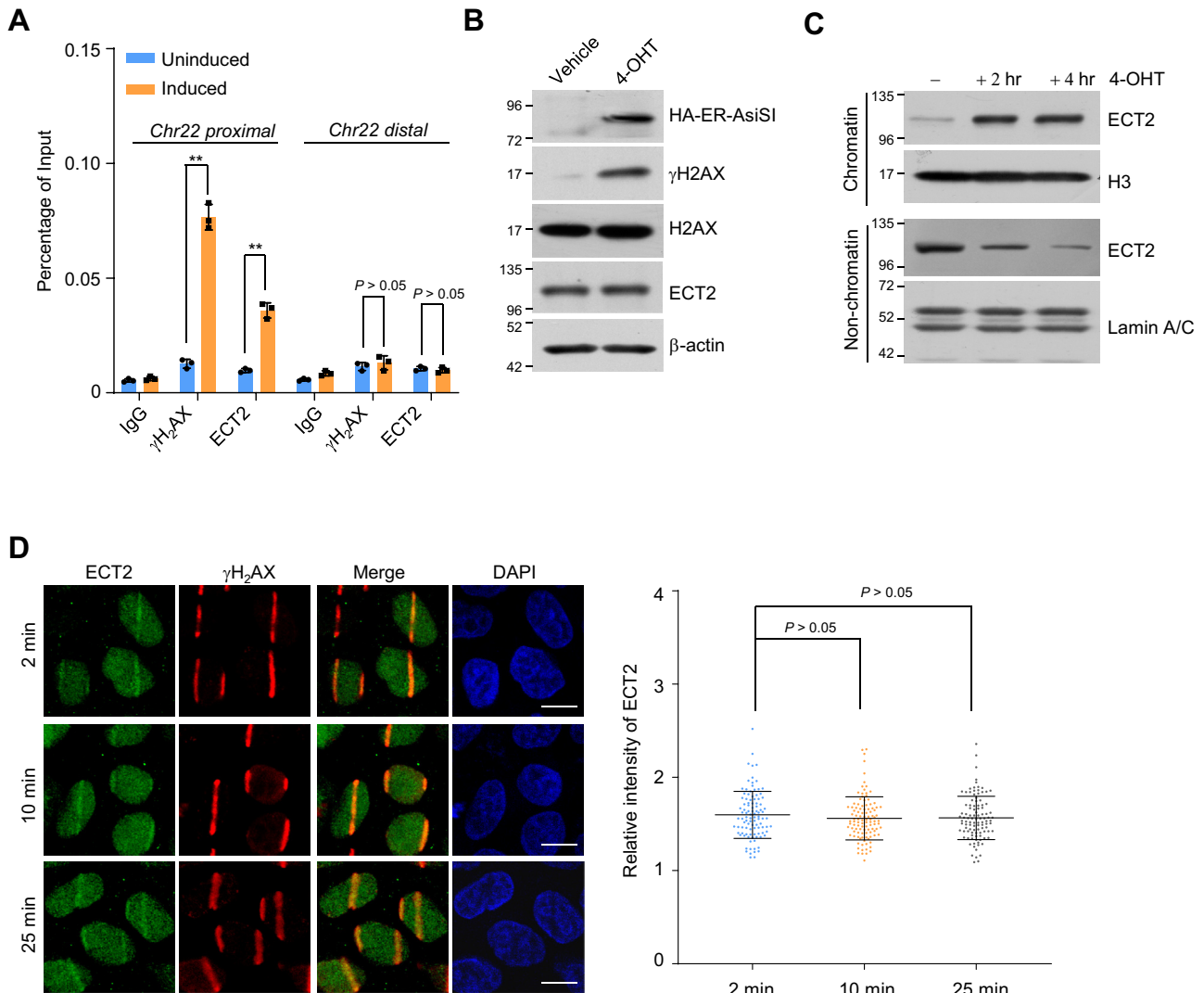
Figure 1. ECT2 is recruited to DNA damage sites. *A*, ECT2 occupancy on chromatin regions that flank DSB generated by the endonuclease AsiSI. ER-AsiSI HeLa cells were treated with vehicle (uninduced) or 4-OHT (induced) for 4 h. Soluble chromatin from these cells was then immunoprecipitated with antibodies against ECT2 or γH2AX. The final DNA extractions were amplified by quantitative real-time PCR using primers that cover the DNA sequences flanking the indicated AsiSI site and the region distal to the DSB. Each bar represents the mean ± SD for biological triplicate experiments. **$p < 0.01$ two-tailed unpaired Student's *t* test. *B*, 4-OHT-induced AsiSI activation and DNA damage were monitored by immunoblotting with the indicated antibodies. *C*, ECT2 is associated with chromatin when DSBs occur. ER-AsiSI HeLa cells were treated with vehicle or 4-OHT for 2 or 4 h. Nuclear proteins were extracted and fractionated followed by immunoblotting analysis with the indicated antibodies. *D*, U2OS cells were subjected to laser micro-dissection (355 nm UV) and collected at the indicated time points, followed by immunostaining with antibodies against ECT2 or γH2AX. The intensity of the ECT2 laser stripes visualized by confocal microscopy was quantified and normalized against the nuclear background (n > 100). The scale bar represents 10 μm. The *p* value was determined by the Mann–Whitney U test. 4-OHT, 4-hydroxytamoxifen; γH2AX, phospho-Ser139 on H2AX; DSBs, DNA double-strand breaks; ECT2, epithelial cell transforming sequence 2; ER-AsiSI, estrogen receptor fused to AsiSI.

incomplete copies of the GFP gene was stably integrated into the chromosomal DNA of U2OS cells (Fig. 3*B*). Cleavage of the I-SceI sites restores GFP gene expression through gene conversion–directed HR; the efficiency of HR repair is reflected by the percentage of cells expressing GFP protein. The results showed that the proportion of GFP-positive cells was significantly lower in ECT2-depleted cells (Fig. 3*B*), indicating that ECT2 is required for HR repair of DSBs. Immunoblotting confirmed that ECT2 expression was knocked down after siRNA treatment (Fig. 3*B*). In agreement with our results showing that ECT2 has a key role in HR, we used EdU-positive staining to show that ECT2 is highly expressed in S phase cells (Fig. S3*A*). At the time of analysis, knockdown of ECT2 did not

significantly alter the cell-cycle profiles (Fig. S3*B*), suggesting defects in HR induced by decreases in ECT2 expression are not due to cell-cycle redistribution.

Next, we asked whether the GEF activity of ECT2 is required for DSB repair. Endonuclease I-SceI and ECT2 siRNA were transfected into reporter cells stably expressing siRNA-resistant WT ECT2 (ECT2/wt) or a GEF activity-defective ECT2 mutant (ECT2/GEF^mt, E428A, and N608A within the DH domain) (33, 39). FACS analysis revealed that ECT2/wt and ECT2/GEF^mt promoted NHEJ repair with comparable efficacy in ECT2-depleted cells (Fig. 3*C*). Similar observations were obtained when this strategy was used in DR-GFP U2OS cells to examine HR efficiency (Fig. 3*D*). The knockdown and
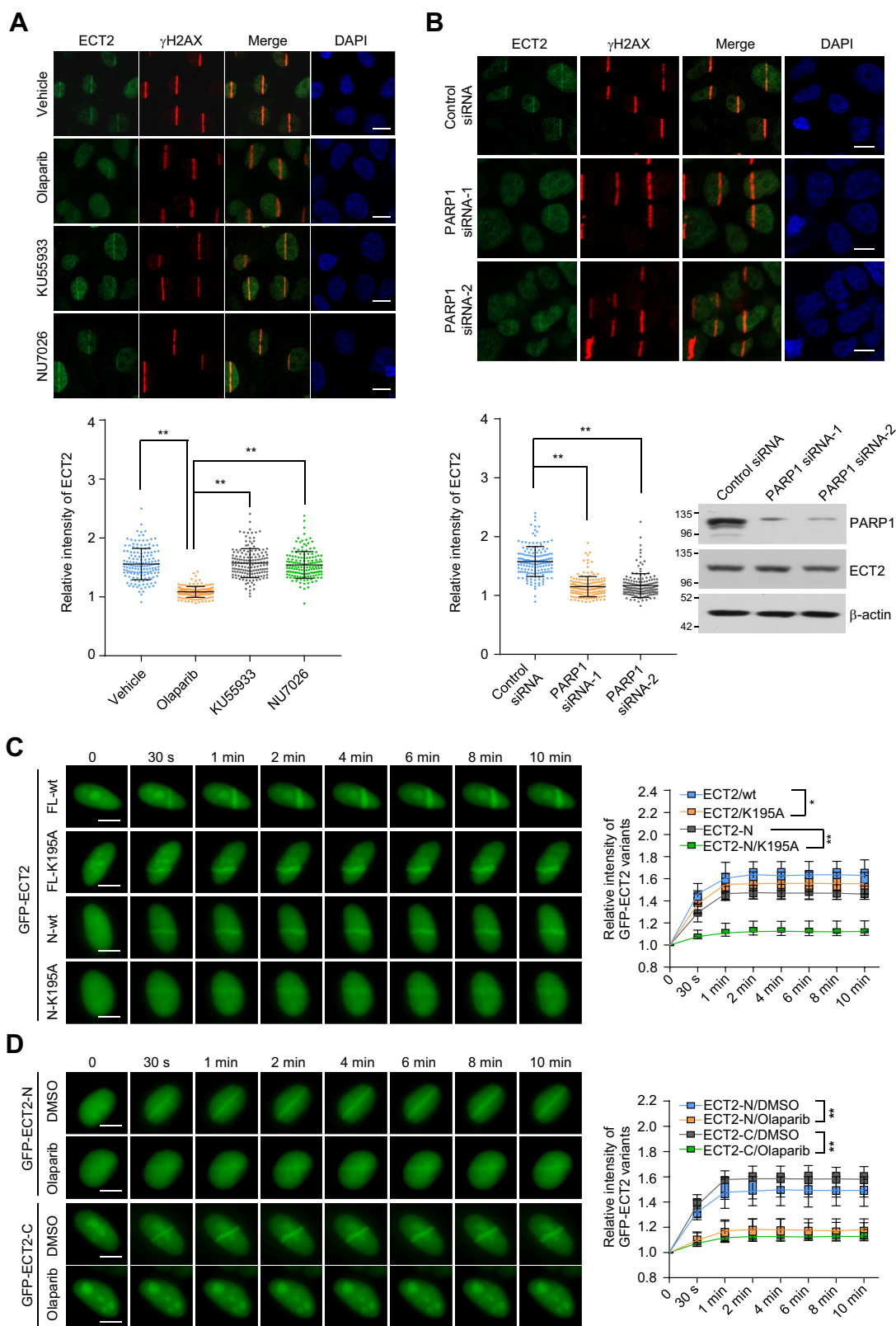
Figure 2. PARP1 controls the recruitment of ECT2. *A*, analysis of endogenous ECT2 recruitment in U2OS cells treated with different inhibitors and subjected to laser microdissection and immunostaining. Cells were pretreated with the PARP1 inhibitor olaparib (10 μM), the ATM inhibitor KU55933 (10 μM), or the DNA-PKcs inhibitor NU7026 (10 μM) for 4 h and then collected at 10 min after irradiation and immunostained with antibodies against ECT2 or γH2AX. The intensity of the ECT2 laser stripes was quantified and normalized against the nuclear background (n > 150). Each bar represents the mean ± SD of biological triplicate experiments. **$p < 0.01$, Mann–Whitney U test. The scale bar represents 10 μm. *B*, analysis of endogenous ECT2 recruitment in PARP1-depleted U2OS cells subjected to laser microdissection and immunostaining. Cells were transfected with control or PARP1 siRNAs for 72 h and collected at 10 min after irradiation and immunostained with antibodies against ECT2 or γH2AX. The intensity of ECT2 laser stripes was quantified and normalized against the nuclear background (n > 150). Each bar represents the mean ± SD of biological triplicate experiments. **$p < 0.01$, Mann–Whitney U

overexpression of ECT2 were monitored by immunoblotting (Fig. 3, *C* and *D*). Knockdown of CDC42 or RAC1, two nuclear Rho-GTPases targeted by ECT2, did not markedly affect HR and NHEJ repair (Fig. S3, *C–E*). We found that both ECT2/wt and ECT2/GEF^{mt} were effectively recruited to DNA lesions (Fig. 3*E*). Collectively, these results support the notion that the GEF activity of ECT2 is not involved in DSB repair.

ECT2 is associated with BRCA1 and KU proteins

To understand the molecular mechanisms by which ECT2 promotes DSB repair, we next examined the ECT2-containing protein complex. First, whole-cell extracts from HeLa cells stably expressing FLAG-ECT2 were purified with an anti-FLAG affinity column. After extensive washing, the bound proteins were eluted with excess FLAG peptides, resolved, and visualized by silver staining on SDS-PAGE. MS analysis of FLAG-ECT2–containing protein complexes recovered from the gel bands revealed that ECT2 associated with several DDR proteins, including PARP1, BRCA1, and KU proteins (Fig. 4*A*, Fig. S4*A*, and Supplementary File 1). Coimmunoprecipitation analysis demonstrated that BRCA1, KU70, KU80, and PARP1, but not RAD50 (one of the constitutive components of the MRN complex), was immunoprecipitated with ECT2 (Fig. 4*B*). Reciprocal experiments showed that ECT2 was precipitated by KU70, KU80, and BRCA1 (Fig. S4*B*).

To evaluate whether the association of ECT2 with BRCA1, KU70, and KU80 was indirectly linked by DNA molecules, cellular extracts from FLAG-ECT2–expressing cells were pretreated with DNase followed by coimmunoprecipitation analysis. The results indicated that DNase treatment did not affect the association between ECT2 and these DDR factors (Fig. 4*C*). Also, the mutation of GEF (ECT2/GEF^{mt}) and the K195A mutation did not affect the association of ECT2 with these factors (Fig. 4*D*). To gain molecular insights into the ECT2-associated protein complexes, FLAG-tagged ECT2 truncations were generated and transfected into HeLa cells. Coimmunoprecipitation analysis demonstrated that the fragment of ECT2 containing the N-terminal BRCT domains was specifically responsible for the association of ECT2 with BRCA1, KU70, and KU80 (Fig. 4*E*). Collectively, these results indicated that the N-terminal region of ECT2 associates with BRCA1 and KU proteins.

ECT2 facilitates the assembly of BRCA1 and KU70 on damaged chromatin

To gain further mechanistic insights into the role of ECT2 in DSB repair, we then asked if ECT2 can influence the assembly of key DDR proteins on damaged chromatin. First, we assessed the accumulation of MDC1 at DSB sites in ER-AsiSI HeLa cells. Immunostaining and confocal microscopy analysis

demonstrated that a reduction in ECT2 expression did not alter the formation of MDC1 foci (Fig. S5*A*). The level of conjugated ubiquitin, which is produced by E3 ligases RNF8 and RNF168, was not affected by a reduction in ECT2 expression (Fig. S5*A*). We then analyzed IR-induced focus formation of γH2AX, 53BP1, and BRCA1 in ECT2-depleted cells. The results showed that the accumulation of BRCA1 at damaged sites was significantly reduced (Fig. 5*A*), but the IR-induced foci of γH2AX and 53BP1 were largely unaffected (Fig. S5*B*). Importantly, we demonstrated that either ECT2/wt or ECT2/GEF^{mt} compensated for defective BRCA1 engagement on damaged chromatin in ECT2-depleted and EdU-positive cells (Fig. 5*A*). Reciprocal experiments showed BRCA1 knockdown only marginally affected on ECT2 recruitment (Fig. S5*C*). We then examined the IR-induced foci of RAD51, a DNA recombinase that acts downstream of BRCA1 in HR repair, and found RAD51 accumulation on damaged chromatin is also controlled by ECT2 independently of GEF activity (Fig. 5*B*). The expression of BRCA1 and RAD51 was not affected by ECT2 knockdown or overexpression (Fig. S5*D*). These results suggest that ECT2 promotes HR repair of DSBs by facilitating BRCA1 recruitment to damaged chromatin.

To assess how ECT2 is involved in NHEJ repair, we then monitored the recruitment of KU70 after laser micro-IR in U2OS cells expressing GFP-KU70. Microscopy and live-cell imaging analysis showed that ECT2 depletion impaired the recruitment of KU70 (Fig. 5*C* and Fig. S5*E*), but KU70 knockdown did not alter the formation of laser stripes by ECT2 (Fig. S5*F*). In agreement with the observations from NHEJ reporter assays, we found that defective KU70 recruitment in ECT2-depleted cells was restored by expression of either ECT2/wt or ECT2/GEF^{mt} (Fig. 5*C*). These results imply that ECT2 promotes NHEJ repair of DSBs by facilitating KU70 recruitment to damaged chromatin.

ECT2 protects cells from DNA damage

The above findings prompted us to ask whether ECT2 plays a role in genome stability. To investigate this, we first analyzed the ability of ECT2-knockdown cells to recover from DNA damage. In ECT2-deficient cells, γH2AX foci persisted 24 h after the IR challenge but had largely disappeared in ECT2-proficient cells (Fig. 6*A*). Next, comet assays showed that ECT2 depletion caused significant DNA damage after IR exposure, as evidenced by an increase in the length of the comet tail. ECT2/wt or ECT2/GEF^{mt} overexpression decreased the comet tail length in ECT2-deficient cells (Fig. 6*B*). These results suggest that the expression of ECT2 is crucial for cells to repair damaged DNA, and thus, ECT2 regulates genome stability.

---

test. The scale bar represents 10 μm. *C*, laser micro-IR (70% of full power) followed by live-cell imaging analysis of the recruitment of GFP-ECT2 variants in U2OS cells. The fluorescence intensity in microirradiated areas relative to the nuclear background was quantified (n > 15). Data are shown as box plots from biological triplicate experiments. *$p < 0.05$, **$p < 0.01$, two-way ANOVA. The scale bar represents 10 μm. *D*, laser micro-IR (70% of full power) followed by live-cell imaging analysis of the recruitment of GFP-ECT2 truncation mutants in vehicle- or olaparib-treated U2OS cells. The fluorescence intensity in microirradiated areas relative to the nuclear background was quantified (n > 15). Data are shown as box plots from biological triplicate experiments. **$p < 0.01$, two-way ANOVA. The scale bar represents 10 μm. γH2AX, phospho-Ser139 on H2AX; DNA-PKcs, DNA–protein kinase; ECT2, epithelial cell transforming sequence 2; PARP1, poly(ADP-ribose) polymerase 1.
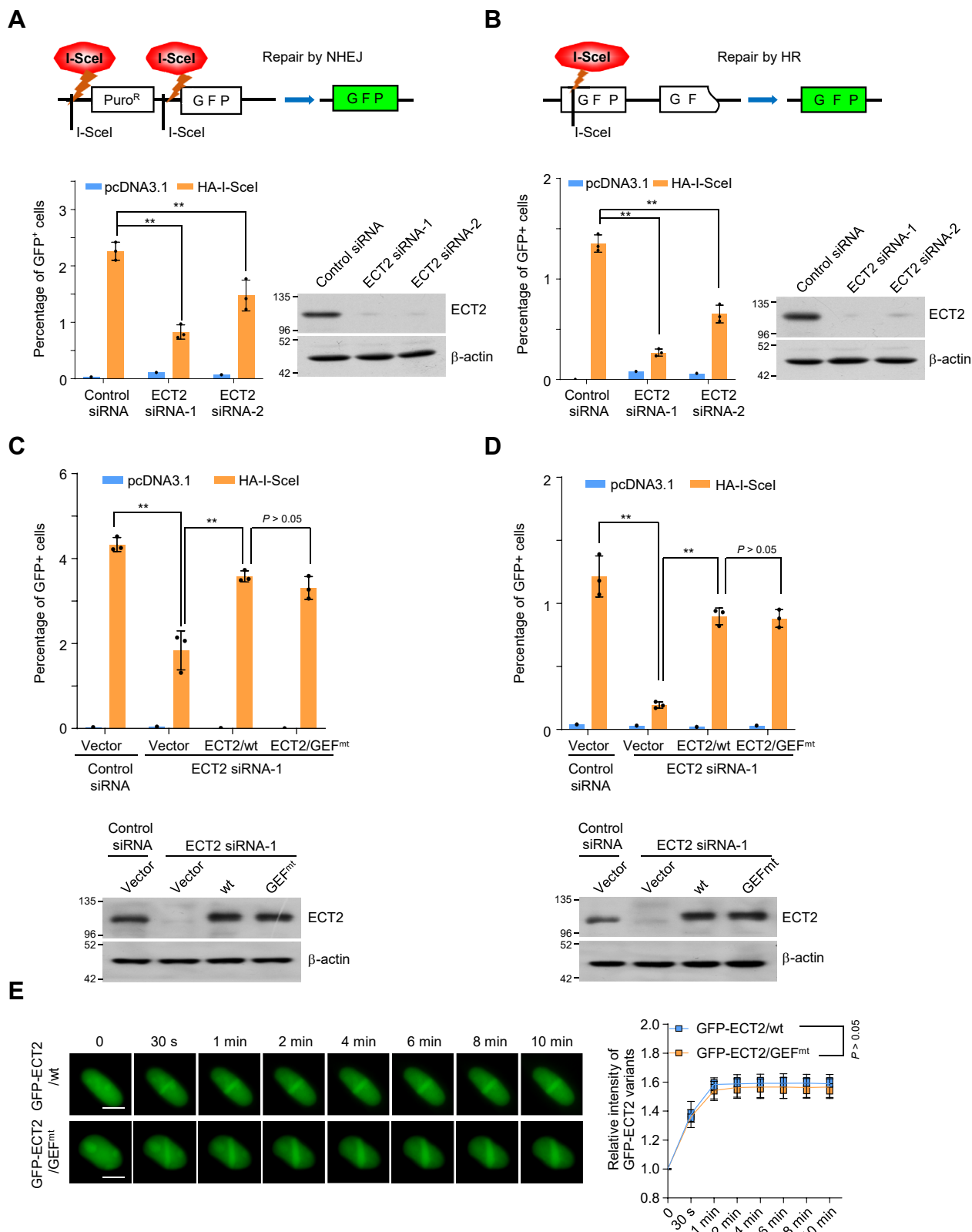
Figure 3. ECT2 is required for efficient HR and NHEJ. *A*, examination of NHEJ efficiency in ECT2-depleted U2OS reporter cells. The GFP-positive cell fraction was determined by flow cytometry. A schematic representation of the NHEJ reporter construct is shown; the knockdown effect was examined by immunoblotting. Each bar represents the mean ± SD for biological triplicate experiments. **p < 0.01, one-way ANOVA. *B*, examination of HR efficiency in ECT2-depleted DR-GFP U2OS reporter cells. The GFP-positive cell fraction was determined by flow cytometry. A schematic representation of the HR reporter construct is shown; the knockdown effect was examined by immunoblotting. Each bar represents the mean ± SD for biological triplicate experiments. **p < 0.01, one-way ANOVA. *C*, examination of NHEJ efficiency in U2OS reporter cells stably expressing ECT2 variants; cells were transfected with control or ECT2 5′UTR siRNA (ECT2 siRNA-1) followed by flow cytometry analysis. Cellular extracts from these cells were examined by immunoblotting. Each bar represents the mean ± SD of biological triplicate ceperiments. **p < 0.01, one-way ANOVA. *D*, DR-GFP U2OS reporter cells stably expressing ECT2 variants were

To further assess the role of ECT2 in protecting genome integrity, we examined the effect of ECT2 deficiency on cell survival after genotoxic insults. Knockdown of ECT2 expression significantly compromised cell survival after IR or etoposide or camptothecin treatment (Fig. 6, C–E). Expression of either ECT2/wt or ECT2/GEF^{mt} prevented the reduced cell survival associated with ECT2 knockdown (Fig. 6, C–E). Collectively, these data support the notion that ECT2 is a crucial component of the cellular response to DNA damage.

As reported by ourselves and others, ECT2 is a potential oncogene that promotes breast tumorigenesis (35, 40–43). Therefore, we wondered if the high expression level of ECT2 found in breast cancer confers cellular resistance to genotoxic insults. To test this hypothesis, breast cancer cells, including MDA-MB-231 and MCF-7 cells, were transfected with control or ECT2-targeted siRNAs. Survival analysis showed that ECT2-knockdown cells were more vulnerable to IR exposure (Fig. 6, F and G), indicating that high expression of ECT2 may help breast tumor cells manage exogenous DNA damage. This result suggests that ECT2 expression plays a role in the survival of tumor cells.

Discussion

In this study, we revealed that ECT2 acts as an essential caretaker of genome stability by promoting DSB repair. We showed ECT2 controls the accumulation of BRCA1 and KU70 at DSB sites to facilitate HR and NHEJ repair through a mechanism that is independent of its GEF activity. Our study sheds mechanistic light on the nuclear function of ECT2 in DSB repair and uncovers a role of ECT2 in genome maintenance that is not dependent on GEF activity.

In response to DNA damage, BRCT domain–containing proteins form protein complexes generally through distinct pairings of BRCT domains, mediated by phospho-specific or PAR-binding features (44, 45). The N-terminal BRCT domains of ECT2 have high sequence similarities with those of DNA topoisomerase 2–binding protein 1 (which is 40% identical to BRCT1 and 30% identical to BRCT2) (46). In addition, topoisomerase 2–binding protein 1 is an essential regulator of DDR (47, 48), suggesting that the BRCT domains of ECT2 play a role in DDR. Although the recruitment of ECT2 to DNA damage sites was only partially reliant on the BRCT domains, as revealed by experiments using laser micro-IR and an ECT2 truncation mutant or point mutant, we demonstrated that the BRCT domains are responsible for the association of ECT2 with BRCA1 and KU proteins. These results imply that the BRCT domains of ECT2 have several roles in DSB repair. Future studies are needed to reveal how ECT2 mediates the assembly of BRCA1 and KU proteins on damaged chromatin. It is possible that ECT2 binds directly to and recruits these factors *via* BRCT domains, or ECT2 may indirectly alter the conformation of

damaged chromatin by reading certain (as yet undefined) chromatin modifications, or ECT2 may scaffold chromatin remodeling complexes. Our data demonstrated a mechanism for ECT2 activity that differs from the canonical phosphorylation-dependent recruitment of BRCT domain–containing proteins; our results showed ECT2 enrichment at DNA damage sites depends on the PARylation of several multiple distinct regions of ECT2, including BRCTs and the C terminus. We believe that further characterization of the PARylation sites and/or the PAR-binding activity of the C terminus of ECT2 will help us better understand the molecular mechanism of ECT2 recruitment and its activity in DSB repair.

ECT2 is involved in many cellular processes including cell division, growth, polarity, adhesion, migration, and centromere maintenance (26, 28, 32). In addition to its N-terminal domains (49, 50), the activity of ECT2 can be autoinhibited by the C-terminal PH domain, which can fold and block the canonical RhoA-binding site at the catalytic center of the DH domain (26). During cytokinesis, ECT2 localized at the division plane of the plasma membrane changes from an inactive state to an active state through allosteric regulation by RhoA (26), and ECT2 activation in turn activates RhoA to mediate a positive-feedback loop (51). Nearly all functions of ECT2 reported to date involve GEF activity (28). However, we revealed that the GEF catalytic activity of ECT2 is dispensable for ECT2-promoted DSB repair, evidenced by compensation assays with a GEF-defective mutant in ECT2-knockdown cells. In support of this finding, depletion of either CDC42 or RAC1, two nuclear Rho-GTPases targeted by ECT2, had only a minor effect on HR and NHEJ repair. Although the molecular mechanisms of GEF-independent activity remain to be investigated, we propose that either the autoinhibited form of ECT2 or the activated conformation of ECT2 could efficiently assemble DNA repair machinery. Evidence for this proposal comes from the observation that either ECT2/wt or ECT2/GEF^{mt} associated with BRCA1 and KU70 and promoted the engagement of these factors at DSB sites.

It was reported that Ect2 knockdown in doxorubicin-treated primary mouse embryonic fibroblasts did not significantly alter the recruitment of BRCA1 to DNA lesions (34). Yet, we showed that ECT2 depletion in human cells impaired the formation of IR-induced BRCA1 foci, and rescue experiments indicated that forced expression of ECT2 reversed this impairment. In He's study (34), knockdown of Ect2 in mouse embryonic fibroblasts reduced damage-induced apoptosis. This finding is also inconsistent with our observations that ECT2-deficient cells were hypersensitive to genotoxic insults. The discrepancies between our study and that of He *et al.* may come from the use of different cell systems.

Increasing evidence, including our previous study, indicates that dysregulated ECT2 activity is implicated in many types of cancer and that ECT2 depletion suppresses tumorigenesis (35,

transfected with control or ECT2 5′UTR siRNA followed by flow cytometry analysis. Cellular extracts from these cells were examined by immunoblotting. Each bar represents the mean ± SD of biological triplicate experiments. **p < 0.01, one-way ANOVA. *E*, laser micro-IR (70% of full power) followed by live-cell imaging analysis of the recruitment of GFP-ECT2 variants recruitment in U2OS cells. The fluorescence intensity in microirradiated areas relative to the nuclear background was quantified (n > 15). Data are shown as box plots from biological triplicate experiments. The p value was determined by two-way ANOVA. The scale bar represents 10 μm. ECT2, epithelial cell transforming sequence 2; HR, homologous recombination; NHEJ, nonhomologous end joining.
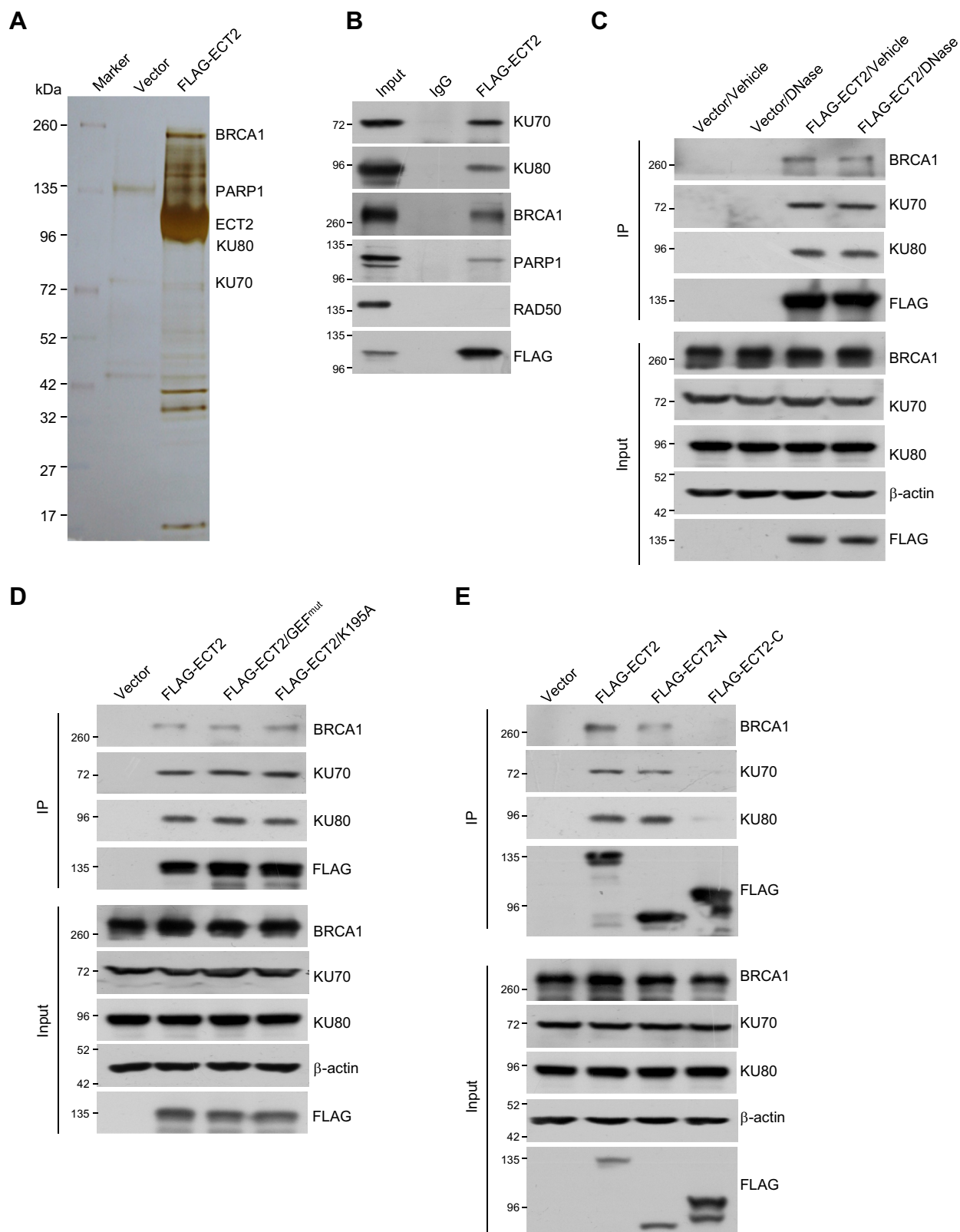
Figure 4. ECT2 is associated with BRCA1 and KU proteins. *A*, immunopurification and MS analysis of ECT2-containing protein complex. Cellular extracts from HeLa cells expressing FLAG-ECT2 were immunopurified with anti-FLAG affinity beads and eluted with FLAG peptide. The eluates were resolved on SDS/PAGE followed by silver staining and MS analysis. *B*, whole-cell lysates from HeLa cells expressing FLAG-ECT2 were immunoprecipitated and immunoblotted with antibodies against the indicated proteins. *C*, whole-cell lysates from HeLa cells expressing FLAG-GFP-ECT2 were immunoprecipitated and immunoblotted with antibodies against the indicated proteins. Cellular extracts were incubated with or without DNase before immunoprecipitation. *D*, whole-cell lysates from HeLa cells expressing FLAG-GFP-ECT2 variants were immunoprecipitated and immunoblotted with antibodies against the indicated proteins. *E*, whole-cell lysates from HeLa cells expressing FLAG-GFP-ECT2 or FLAG-GFP-ECT2 truncation mutants were immunoprecipitated and immunoblotted with antibodies against the indicated proteins. ECT2, epithelial cell transforming sequence 2.
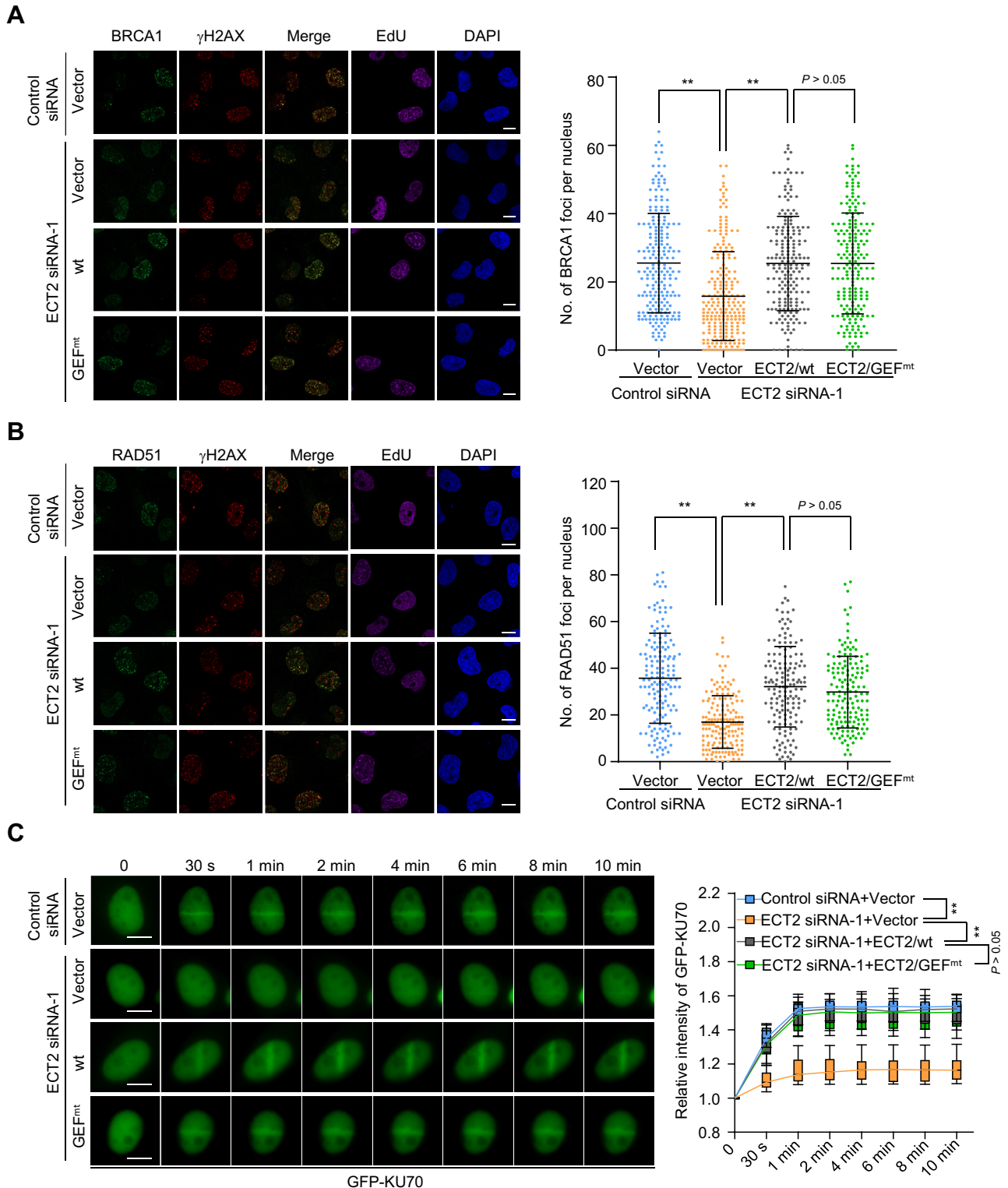
Figure 5. ECT2 facilitates the assembly of BRCA1 and KU70 on damaged chromatin. *A*, examination of BRCA1 focus formation. U2OS cells stably expressing ECT2 variants were transfected with control or ECT2 siRNA. Cells were exposed to IR (4 Gy) and cultured for 3 h followed by 1 h EdU labeling. The fixed cells were then immunostained and analyzed by confocal microscopy. The number of BRCA1 foci per cell after each treatment was quantified (n > 200). Each bar represents the mean ± SD for biological triplicate experiments. **$p < 0.01$, Mann–Whitney test. The scale bar represents 10 μm. *B*, examination of RAD51 focus formation. U2OS cells stably expressing ECT2 variants were transfected with control or ECT2 siRNA. Cells were exposed to IR (4 Gy) and cultured for 3 h followed by 1 h EdU labeling. The fixed cells were then immunostained and analyzed by confocal microscopy. The number of RAD51 foci per cell after each treatment was quantified (n > 150). Each bar represents the mean ± SD for biological triplicate experiments. **$p < 0.01$, Mann–Whitney U test. The scale bar represents 10 μm. *C*, examination of KU70 recruitment. U2OS cells stably expressing ECT2 variants were transfected with GFP-KU70 and either control or ECT2 siRNA. Cells were then subjected to laser micro-IR (70% of full power) followed by live-cell imaging analysis. The fluorescence intensity in microirradiated areas relative to the nuclear background was quantified (n > 15). Data are shown as box plots from biological triplicate experiments. **$p < 0.01$, two-way ANOVA. The scale bar represents 10 μm. ECT2, epithelial cell transforming sequence 2; IR, irradiation.
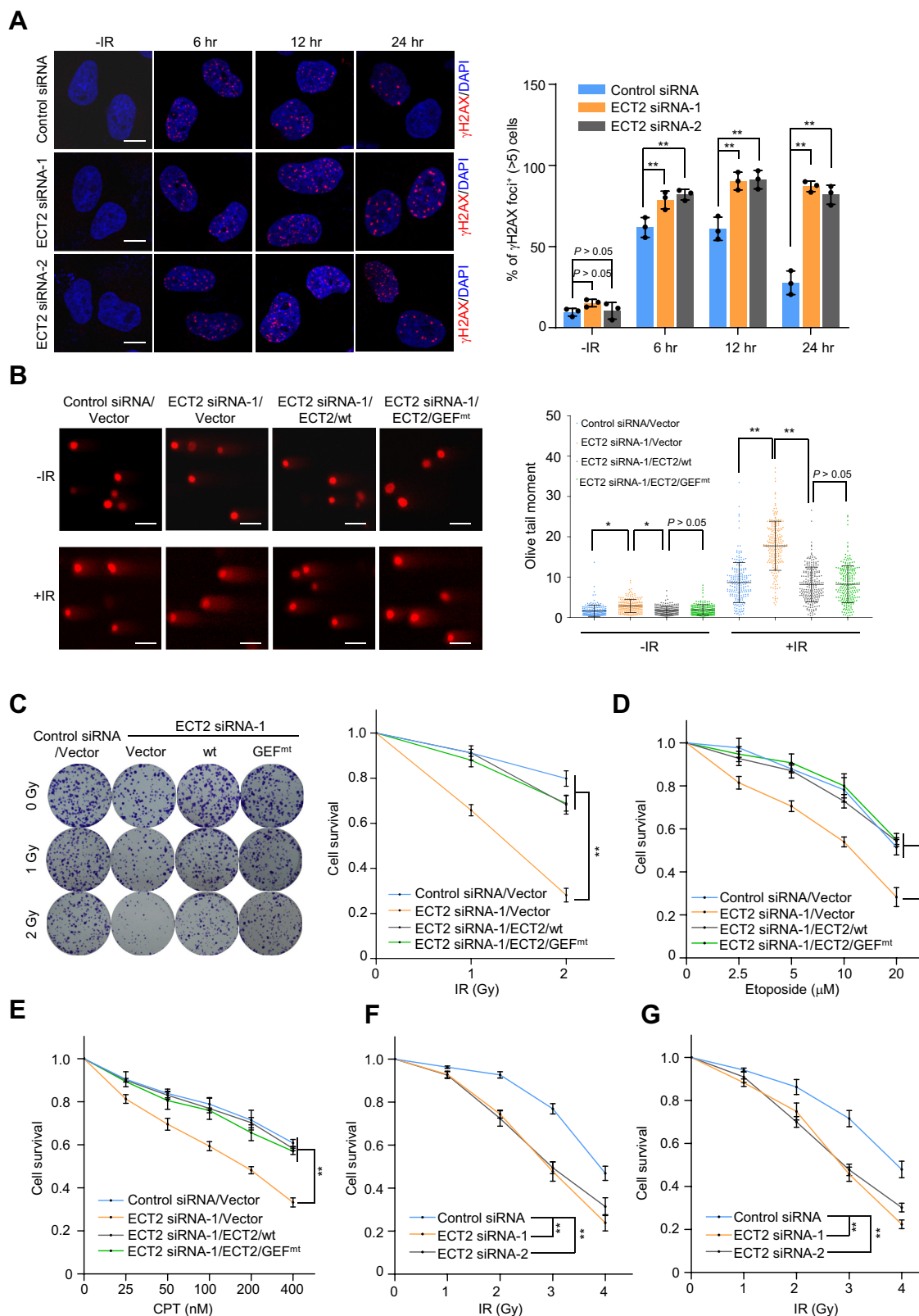
Figure 6. ECT2 protects cells from DNA damage. *A*, U2OS cells in which ECT2 was knocked down were exposed to IR (4 Gy) for the indicated time points followed by γH2AX staining and confocal microscopy analysis. The number of γH2AX foci per cell after each treatment was quantified (n > 100). Each bar represents the mean ± SD for biological triplicate experiments. **$p < 0.01$, one-way ANOVA. The scale bar represents 10 μm. *B*, the accumulation of damaged DNA was examined and quantified using the neutral comet assay. U2OS cells stably expressing ECT2 variants were transfected with control or ECT2 siRNA, and cells were challenged with 4 Gy IR. The tail formation in each treatment was quantified (n > 180). Each bar represents the mean ± SD of biological triplicate experiments. *$p < 0.05$, **$p < 0.01$, Mann–Whitney U test. The scale bar represents 50 μm. *C*, survival analysis of U2OS cells expressing ECT2 5′UTR siRNA and ECT2 variants treated with varying doses of IR followed by colony-formation assays. The colony numbers were counted, and representative images are shown. Each bar represents the mean ± SD of biological triplicate experiments. **$p < 0.01$, two-way ANOVA. *D*, survival analysis of

41, 52, 53). These findings suggest that ECT2 acts as an oncogenic protein. Tumor cells contain high levels of replication stress–associated DNA damage, and the resolution of this damage depends heavily on HR repair to maintain cell survival (54, 55). Based on this knowledge and our results, we propose that overexpression of ECT2 in cancer cells promotes DSB repair, which helps cancer cells overcome endogenous DNA damage, promoting their survival and driving tumorigenesis. In addition, ECT2 inhibition may enhance the therapeutic efficacy of radiotherapy or chemotherapy.

Experimental procedures

Antibodies and reagents

The sources of antibodies against the following proteins were as follows: ECT2 (07-1364, for Western blotting [WB], ChIP, and IF) and γH2AX (05-636, for IF and WB) were purchased from Millipore; poly(ADP-ribose) (ALX-840-220-R100, for IF) was purchased from ENZO; HA (sc-805, for WB) and PARP1 (sc-7150 for WB) were purchased from Santa Cruz Biotechnology; β-actin (AC026, for WB) was purchased from ABclonal; FLAG (F1804, for IP and WB) was purchased from Sigma; RAD51 (ab63801, for IF and WB) and RAD50 (ab89, for WB) were purchased from Abcam; BRCA1 (22362-1-AP, for IF and WB), KU70 (10723-1-AP, for WB), and KU80 (16389-1-AP, for WB) were purchased from Proteintech; H3 (YM3038, for WB), H2AX (YT2155, for WB), and LaminA/C (YT2521, for WB) were purchased from ImmunoWay. Anti-FLAG M2 affinity gel (A2220), 3× FLAG peptide (F4799), puromycin (P8833), 4-OHT (H6278), KU55933 (SML1109), and NU7026 (N1537) were purchased from Sigma. Olaparib (S1060) was purchased from Selleck. MNNG (70-25-7) was purchased from Tokyo Chemical Industry.

Plasmids

The FLAG-ECT2 plasmid was amplified from ECT2 cDNA (Open BioSystems) and cloned into a pLenti-puro or pLenti-puro-GFP vector. FLAG-ECT2, FLAG-ECT2-N (1–424), and FLAG-ECT2-C (425–883) carried by the pLenti-puro-GFP vector were generated by standard cloning procedures. ECT2/GEF^mt, ECT2/K195A, and ECT2-N/K195A were generated by quick-change point mutation assays. GFP-KU70 or GFP-KU80 was amplified from KU70 or KU80 cDNA, respectively (Open BioSystems) and cloned into a pLenti-Neo-GFP vector. FLAG-BRCA1 was amplified from BRCA1 cDNA (Open Biosystems) and cloned into a pcDNA3.1 vector.

Cell culture

U2OS, MCF-7, HeLa, HEK293T, and MDA-MB-231 cells were purchased from the American Type Culture Collection and cultured according to the supplier's instructions. All of the cells were authenticated by examination of morphology and growth characteristics and were confirmed free of *Mycoplasma*.

ChIP

ChIP experiments were performed according to the procedure described previously (56). About 10 million cells were cross-linked with 1% formaldehyde for 10 min at room temperature (RT) and quenched by the addition of glycine for 5 min at a final concentration of 125 mM. The fixed cells were resuspended in SDS lysis buffer (1% SDS, 5 mM EDTA, and 50 mM Tris HCl, pH 8.1) in the presence of protease inhibitors and subjected to 30 cycles (30 s on and 30 s off) of sonication (Bioruptor, Diagenode) to generate chromatin fragments 300 bp in length. Lysates were diluted in a buffer containing 1% Triton X-100, 2 mM EDTA, 20 mM Tris HCl, pH 8.1, and 150 mM NaCl. For immunoprecipitation, the diluted chromatin was incubated with control or specific antibodies (2 μg) for 12 h at 4 °C with constant rotation; 50 μl of 50% (v/v) protein G magnetic beads was added, and then, the incubation was continued for 2 h. Beads were then washed with the following buffers: TSE I (0.1% SDS, 1% Triton X-100, 2 mM EDTA, 20 mM Tris HCl, pH 8.1, and 150 mM NaCl); TSE II (0.1% SDS, 1% Triton X-100, 2 mM EDTA, 20 mM Tris HCl, pH 8.1, and 500 mM NaCl); buffer III (0.25 M LiCl, 1% Nonidet P-40, 1% sodium deoxycholate, 1 mM EDTA, and 10 mM Tris-HCl, pH 8.1); and Tris/EDTA buffer. The beads were collected between washes using a magnetic stand at 4 °C. Then, the cross-linking of pulled-down chromatin complex together with the input was inhibited at 70 °C for 2 h in the elution buffer (1% SDS, 5 mM EDTA, 20 mM Tris HCl, pH 8.1, 50 mM NaCl, and 0.1 mg/ml proteinase K). Eluted DNA was purified with a PCR purification kit (Qiagen) and analyzed by quantitative PCR using the following primers; Chr22 proximal forward: CCTTCTTTCCCAGTGGTTCA, reverse: GTGGTCTGACCCAGAGTGGT; Chr22 distal forward: CCCATCTCAACCTCCACACT, reverse: CTTGTCCAGATTCGCTGTGA.

Lentiviral production

The vectors encoding ECT2/wt, ECT2/GEF^mt, and the three assistant vectors pMDLg/pRRE, pRSV-REV, and pVSVG were transiently transfected into HEK293T cells. Viral supernatants were collected 48 h later, clarified by filtration, and concentrated by ultracentrifugation. The lentivirus was then infected into cells followed by antibiotic selection to generate stable cells.

Immunoblotting

Whole-cell lysates were harvested from treated cells and then resuspended in 5× SDS-PAGE loading buffer. The boiled protein samples were subjected to SDS-PAGE followed by

---

U2OS cells expressing ECT2 5′UTR siRNA and ECT2 variants treated with etoposide. Each bar represents the mean ± SD of biological triplicate experiments. **$p < 0.01$, two-way ANOVA. *E*, survival analysis of U2OS cells expressing ECT2 5′UTR siRNA and ECT2 variants treated with camptothecin (CPT). Each bar represents the mean ± SD for biological triplicate experiments. **$p < 0.01$, two-way ANOVA. *F*, survival analysis of IR-treated MDA-MB-231 cells expressing control or ECT2 siRNAs. Each bar represents the mean ± SD of biological triplicate experiments. **$p < 0.01$, two-way ANOVA. *G*, survival analysis of IR-treated MCF-7 cells expressing control or ECT2 siRNAs. Each bar represents the mean ± SD of biological triplicate experiments. **$p < 0.01$, two-way ANOVA. γH2AX, phospho-Ser139 on H2AX; ECT2, epithelial cell transforming sequence 2; IR, irradiation.

immunoblotting with the appropriate primary and secondary antibodies.

Immunopurification and silver staining

Lysates from HeLa cells stably expressing FLAG-ECT2 were prepared by incubating the cells in the lysis buffer containing a protease inhibitor cocktail (Roche). Anti-FLAG immunoaffinity columns were prepared using anti-FLAG M2 affinity gel following the manufacturer's suggestions. Cell lysates were obtained from about 5×10^8 cells and applied to an equilibrated FLAG column of 1-ml bed volume to allow for adsorption of the protein complex to the column resin. After binding, the column was washed with cold PBS plus 0.2% Nonidet P-40. FLAG peptide was applied to the column to elute the FLAG protein complex following a protocol described by the vendor. The eluents were collected and visualized on SDS-PAGE followed by silver staining with a Silver Staining Kit (Pierce). The distinct protein bands were retrieved and analyzed by LC-MS/MS.

MS analysis and data processing

The proteins were separated by SDS-PAGE and visualized by silver staining. Then, the corresponding bands were excised and subject to in-gel digestion. The resulting peptides were redissolved in HPLC buffer A (0.1% formic acid in water) after desalting and injected into a Nano-LC system (EASY-nLC 1000, Thermo Fisher Scientific). Peptides were separated using a reversed-phase analytical column and electrosprayed directly into an Orbitrap Q-Exactive mass spectrometer. The mass spectrometric analysis was carried out in a data-dependent mode with an automatic switch between a full MS scan and an MS/MS scan in the orbitrap. For full MS survey scan, automatic gain control target was 1e6 and the scan range was from 350 to 1750 with the resolution of 70, 000. The ten most-intense peaks with charge state 2 and above were selected for fragmentation by higher-energy collision dissociation with normalized collision energy of 27%. The MS2 spectra were acquired with 17,500 resolution. The exclusion duration for the data-dependent scan was 10 s, and the exclusion window was set at 2.2 Da. The resulting MS/MS data were searched using Proteome Discoverer software (v1.4) with an overall false discovery rate for peptides of less than 1%. Proteins demonstrating the score <2 and single-peptide identifications were removed from identification list. Peptide sequences were searched against UniProt human (20,386 entries, downloaded on 2021.06.23) database using trypsin specificity and allowing a maximum of two missed cleavages. Carbamidomethylation on cysteine was specified as fixed modification. Oxidation of methionine and acetylation on peptide N-terminal were set as variable modifications. Mass tolerances for precursor ions were set at ±10 ppm for precursor ions and ±0.02 Da for MS/MS.

RNA interference

All siRNA transfections were performed using Lipofectamine RNAi MAX (Invitrogen) following the manufacturer's recommendations. The final concentration of the siRNA molecules was 10 nM, and cells were harvested 72 or 96 h after transfection depending on the purpose of the experiments. Control siRNA (ON-TARGETplus nontargeting pool, D-001810-10) was purchased from Dharmacon (SMARTpool siRNA) and siRNAs against ECT2 (siRNA-1 targeting 5′ UTR: GGUGGAACUCCUAGGGCUU, siRNA-2 targeting 5′ UTR: CCGGCGAGGAAUGGCGGUA), PARP1 (siRNA-1 targeting 3′UTR: GAGAGAUUCUGUUGCAUAG, siRNA-2 targeting 3′UTR: CGAAGCGCUUCUGCACCAA), BRCA1 (siRNA-1: GGAACCUGUCUCCACAAAG, siRNA-2: GAUAGUUCUACCAGUAAA), KU70 (siRNA-1: GAGUGAAGAUGAGUUGACA, siRNA-2: UUCUCUUGGUAACUUUCCC), CDC42 (AAGAUAACUCACCACUGUCCA), and RAC1 MISSION esiRNA (EHU075591) were chemically synthesized by Sigma.

X-ray IR and laser micro-IR

IR was delivered by an X-ray generator (Rad Source Corporation; RS2000 PRO, 160 kV, 25 mA). Micro-IR was performed with a microscope (Leica) equipped with a 37 °C heating stage and a 365-nm laser diode (Andor Technology). A detectable laser path was generated using a laser setting of 60% or 70% of full power as indicated under a 60× objective lens.

Laser microdissection

Cells were grown on Lab-Tek II chamber slides (Thermo Scientific) in the presence of a phenol red–free medium (Invitrogen) before induction of DNA damage by a UV-A laser (λ = 355 nm, 40% energy) using a Zeiss Observer Z1 inverted microscope with a PALM Microbeam laser microdissection workstation under a 40× objective lens. After IR, the cells were incubated at 37 °C before being processed for immunostaining.

Immunofluorescence

Cells on glass coverslips (BD Biosciences) were fixed with 4% paraformaldehyde and permeabilized with 0.2% Triton X-100 in PBS. Samples were blocked in 5% donkey serum in the presence of 0.1% Triton X-100 and stained with the appropriate primary antibodies and secondary antibodies coupled to Alexa Fluor 488 or Alexa Fluor 594 (Thermo Fisher). Confocal images were captured on a Zeiss LSM800 microscope using a 63× oil objective. To avoid bleed-through effects in double-staining experiments, each dye was scanned independently in a multitracking mode.

Comet assay

The CometAssay kit (Trevigen) was used to monitor damaged DNA according to the manufacturer's instructions. Briefly, cells were resuspended in ice-cold PBS at a concentration of 1×10^5 cells/ml. Cells (5 μl) were mixed with 50 μl of warm low-melting agarose and evenly spread onto the comet slides. Slides were then incubated in a prechilled lysis solution for 60 min at 4 °C. Next, the slides were treated with neutral unwinding solution for 60-min incubation at RT. The slides

were transferred to an electrophoresis tank, which contained a prechilled neutral electrophoresis solution, and the system was run at 1 V/cm, 300 mA, for 30 min at 4 °C. The slides were immersed twice in deionized water for 5 min and washed in 70% ethanol for 5 min. Cells were then stained with 100 μl propidium iodide for 20 min in the dark and analyzed using an Olympus IX71 inverted fluorescence microscope. Comet tails were analyzed using CaspLab software followed by statistical analysis.

Flow cytometry analysis

To analyses the cell-cycle distribution, cells were treated with 10 μM EdU for 1 h and labeled using a Click-iT EdU Alexa Fluor 647 flow cytometry assay kit according to the manufacturer's instructions (Keygen Technology). For each sample, 1×10^6 cells were fixed in cold ethanol, treated with RNase A, stained with propidium iodide, and analyzed on a BD Biosciences FACSCalibur.

Cell survival assay

Cells were plated into 96-well plates at a density of 2000 cells/well. After 24 h, cells were treated with various doses of genotoxic agents for 72 h. Then, CellTiter AQueous One Solution (G3582, Promega) was added to each well according to the manufacturer's instructions, and cell survival was determined after 1 h incubation by measuring the absorbance at 490 nm using a Bio-Rad plate reader (model 550; Bio-Rad).

HR and NHEJ reporter assays

HR or NHEJ efficiency was examined with DR-GFP or EJ5 U2OS cells. In these cells, two incomplete copies of the GFP gene are stably integrated into the chromosomal DNA; cleavage of the I-SceI sites restores GFP gene expression through HR or NHEJ. The percentage of GFP-positive cells was counted by flow cytometry analysis using an Accuri C6 flow cytometer (BD Biosciences). A minimum of 10,000 cells was collected for each treatment and analyzed with FlowJo software.

Colony formation assay

Cells were treated with the indicated conditions and then maintained in culture media for 14 days. After 14 days, the cells were washed with PBS, fixed with methyl alcohol for 10 min, and stained with crystal violet (0.5% wt/vol) for 20 min. The number of colonies per well was counted.

Statistical analysis

Data from biological triplicate experiments are presented as the mean ± SDs. All statistical analyses involved were performed with SPSS 19. Two-tailed, unpaired Student t test was used for comparing two groups of data. ANOVA with Bonferroni's correction was used to compare multiple groups of data. $p < 0.05$ was considered statistically significant. Before statistical analysis, variation within each group of data and the assumptions of the tests were checked. For values not normally distributed, the Mann–Whitney U test was used.

Data availability

All relevant data are available from the authors on request. The mass spectrometry proteomics data have been deposited to the ProteomeXchange Consortium (http://proteomecentral. proteomexchange.org) *via* the iProX partner repository ([57]) with the dataset identifier PXD026977.

Abbreviations—The abbreviations used are: 4-OHT, 4-hydroxytamoxifen; γH2AX, phospho-Ser139 on H2AX; BRCA1, breast cancer type 1; BRCT, BRCA1 C-terminal; CDC42, cell division cycle 42; ChIP, chromatin immunoprecipitation; DDR, DNA damage response; DH, Dbl homology; DNA-PKcs, DNA–protein kinase; DSBs, DNA double-strand breaks; ECT2, epithelial cell transforming sequence 2; ER, estrogen receptor; ER-AsiSI, estrogen receptor fused to AsiSI; GEFs, guanine nucleotide exchange factors; HR, homologous recombination; IR, irradiation; K195, lysine 195; MDC1, mediator of DNA damage checkpoint 1; NHEJ, nonhomologous end joining; PAR, poly-ADP ribose; PARP1, poly(ADP-ribose) polymerase 1; PARylation, poly(ADP-ribosyl)ation; PH, pleckstrin homology; RAC1, Rac family small GTPase 1; Rho, Ras homologous; RhoA, Ras homolog family member A; WB, Western blotting.

References

1. Aguilera, A., and Gómez-González, B. (2008) Genome instability: A mechanistic view of its causes and consequences. *Nat. Rev. Genet.* **9**, 204–217
2. Misteli, T., and Soutoglou, E. (2009) The emerging role of nuclear architecture in DNA repair and genome maintenance. *Nat. Rev. Mol. Cell Biol.* **10**, 243–254
3. Peterson, C. L., and Cote, J. (2004) Cellular machineries for chromosomal DNA repair. *Genes Dev.* **18**, 602–616
4. Chapman, J. R., Taylor, M. R., and Boulton, S. J. (2012) Playing the end game: DNA double-strand break repair pathway choice. *Mol. Cell* **47**, 497–510
5. Schwertman, P., Bekker-Jensen, S., and Mailand, N. (2016) Regulation of DNA double-strand break repair by ubiquitin and ubiquitin-like modifiers. *Nat. Rev. Mol. Cell Biol.* **17**, 379–394

6. Clouaire, T., and Legube, G. (2015) DNA double strand break repair pathway choice: A chromatin based decision? *Nucleus* **6**, 107–113

7. Chang, H. H. Y., Pannunzio, N. R., Adachi, N., and Lieber, M. R. (2017) Non-homologous DNA end joining and alternative pathways to double-strand break repair. *Nat. Rev. Mol. Cell Biol.* **18**, 495–506

8. Myler, L. R., Gallardo, I. F., Soniat, M. M., Deshpande, R. A., Gonzalez, X. B., Kim, Y., Paull, T. T., and Finkelstein, I. J. (2017) Single-molecule imaging reveals how Mre11-Rad50-Nbs1 initiates DNA break repair. *Mol. Cell* **67**, 891–898.e4

9. Scully, R., Panday, A., Elango, R., and Willis, N. A. (2019) DNA double-strand break repair-pathway choice in somatic mammalian cells. *Nat. Rev. Mol. Cell Biol.* **20**, 698–714

10. Li, Z., Li, Y., Tang, M., Peng, B., Lu, X., Yang, Q., Zhu, Q., Hou, T., Li, M., Liu, C., Wang, L., Xu, X., Zhao, Y., Wang, H., Yang, Y., *et al.* (2018) Destabilization of linker histone H1.2 is essential for ATM activation and DNA damage repair. *Cell Res.* **28**, 756–770

11. Seeber, A., and Gasser, S. M. (2017) Chromatin organization and dynamics in double-strand break repair. *Curr. Opin. Genet. Dev.* **43**, 9–16

12. Jacquet, K., Fradet-Turcotte, A., Avvakumov, N., Lambert, J. P., Roques, C., Pandita, R. K., Paquet, E., Herst, P., Gingras, A. C., Pandita, T. K., Legube, G., Doyon, Y., Durocher, D., and Côté, J. (2016) The TIP60 complex regulates bivalent chromatin recognition by 53BP1 through direct H4K20me binding and H2AK15 acetylation. *Mol. Cell* **62**, 409–421

13. Luijsterburg, M. S., de Krijger, I., Wiegant, W. W., Shah, R. G., Smeenk, G., de Groot, A. J. L., Pines, A., Vertegaal, A. C. O., Jacobs, J. J. L., Shah, G. M., and van Attikum, H. (2016) PARP1 links CHD2-mediated chromatin expansion and H3.3 deposition to DNA repair by non-homologous end-joining. *Mol. Cell* **61**, 547–562

14. Savic, V., Yin, B., Maas, N. L., Bredemeyer, A. L., Carpenter, A. C., Helmink, B. A., Yang-Iott, K. S., Sleckman, B. P., and Bassing, C. H. (2009) Formation of dynamic gamma-H2AX domains along broken DNA strands is distinctly regulated by ATM and MDC1 and dependent upon H2AX densities in chromatin. *Mol. Cell* **34**, 298–310

15. Fernandez-Capetillo, O., Chen, H. T., Celeste, A., Ward, I., Romanienko, P. J., Morales, J. C., Naka, K., Xia, Z., Camerini-Otero, R. D., Motoyama, N., Carpenter, P. B., Bonner, W. M., Chen, J., and Nussenzweig, A. (2002) DNA damage-induced G2-M checkpoint activation by histone H2AX and 53BP1. *Nat. Cell Biol.* **4**, 993–997

16. Day, M., Rappas, M., Ptasinska, K., Boos, D., Oliver, A. W., and Pearl, L. H. (2018) BRCT domains of the DNA damage checkpoint proteins TOPBP1/Rad4 display distinct specificities for phosphopeptide ligands. *Elife* **7**, e39979

17. Gerloff, D. L., Woods, N. T., Farago, A. A., and Monteiro, A. N. (2012) BRCT domains: A little more than kin, and less than kind. *FEBS Lett.* **586**, 2711–2716

18. Manke, I. A., Lowery, D. M., Nguyen, A., and Yaffe, M. B. (2003) BRCT repeats as phosphopeptide-binding modules involved in protein targeting. *Science* **302**, 636–639

19. Stucki, M., Clapperton, J. A., Mohammad, D., Yaffe, M. B., Smerdon, S. J., and Jackson, S. P. (2005) MDC1 directly binds phosphorylated histone H2AX to regulate cellular responses to DNA double-strand breaks. *Cell* **123**, 1213–1226

20. Stewart, G. S., Wang, B., Bignell, C. R., Taylor, A. M., and Elledge, S. J. (2003) MDC1 is a mediator of the mammalian DNA damage checkpoint. *Nature* **421**, 961–966

21. Cantor, S. B., Bell, D. W., Ganesan, S., Kass, E. M., Drapkin, R., Grossman, S., Wahrer, D. C., Sgroi, D. C., Lane, W. S., Haber, D. A., and Livingston, D. M. (2001) BACH1, a novel helicase-like protein, interacts directly with BRCA1 and contributes to its DNA repair function. *Cell* **105**, 149–160

22. Cantor, S., Drapkin, R., Zhang, F., Lin, Y., Han, J., Pamidi, S., and Livingston, D. M. (2004) The BRCA1-associated protein BACH1 is a DNA helicase targeted by clinically relevant inactivating mutations. *Proc. Natl. Acad. Sci. U. S. A.* **101**, 2357–2362

23. Chen, L., Nievera, C. J., Lee, A. Y., and Wu, X. (2008) Cell cycle-dependent complex formation of BRCA1.CtIP.MRN is important for DNA double-strand break repair. *J. Biol. Chem.* **283**, 7713–7720

24. Vigil, D., Cherfils, J., Rossman, K. L., and Der, C. J. (2010) Ras superfamily GEFs and GAPs: Validated and tractable targets for cancer therapy? *Nat. Rev. Cancer* **10**, 842–857

25. Hodge, R. G., and Ridley, A. J. (2016) Regulating Rho GTPases and their regulators. *Nat. Rev. Mol. Cell Biol.* **17**, 496–510

26. Chen, M., Pan, H., Sun, L., Shi, P., Zhang, Y., Li, L., Huang, Y., Chen, J., Jiang, P., Fang, X., Wu, C., and Chen, Z. (2020) Structure and regulation of human epithelial cell transforming 2 protein. *Proc. Natl. Acad. Sci. U. S. A.* **117**, 1027–1035

27. Fields, A. P., and Justilien, V. (2010) The guanine nucleotide exchange factor (GEF) Ect2 is an oncogene in human cancer. *Adv. Enzyme Regul.* **50**, 190–200

28. Cook, D. R., Rossman, K. L., and Der, C. J. (2014) Rho guanine nucleotide exchange factors: Regulators of Rho GTPase activity in development and disease. *Oncogene* **33**, 4021–4035

29. Kimura, K., Tsuji, T., Takada, Y., Miki, T., and Narumiya, S. (2000) Accumulation of GTP-bound RhoA during cytokinesis and a critical role of ECT2 in this accumulation. *J. Biol. Chem.* **275**, 17233–17236

30. Justilien, V., Jameison, L., Der, C. J., Rossman, K. L., and Fields, A. P. (2011) Oncogenic activity of Ect2 is regulated through protein kinase C iota-mediated phosphorylation. *J. Biol. Chem.* **286**, 8149–8157

31. Justilien, V., and Fields, A. P. (2009) Ect2 links the PKCiota-Par6alpha complex to Rac1 activation and cellular transformation. *Oncogene* **28**, 3597–3607

32. Lagana, A., Dorn, J. F., De Rop, V., Ladouceur, A. M., Maddox, A. S., and Maddox, P. S. (2010) A small GTPase molecular switch regulates epigenetic centromere maintenance by stabilizing newly incorporated CENP-A. *Nat. Cell Biol.* **12**, 1186–1193

33. Justilien, V., Ali, S. A., Jamieson, L., Yin, N., Cox, A. D., Der, C. J., Murray, N. R., and Fields, A. P. (2017) Ect2-dependent rRNA synthesis is required for KRAS-TRP53-driven lung adenocarcinoma. *Cancer Cell* **31**, 256–269

34. He, D., Xiang, J., Li, B., and Liu, H. (2016) The dynamic behavior of Ect2 in response to DNA damage. *Sci. Rep.* **6**, 24504

35. Zhang, Q., Cao, C., Gong, W., Bao, K., Wang, Q., Wang, Y., Bi, L., Ma, S., Zhao, J., Liu, L., Tian, S., Zhang, K., Yang, J., Yao, Z., Song, N., *et al.* (2020) A feedforward circuit shaped by ECT2 and USP7 contributes to breast carcinogenesis. *Theranostics* **10**, 10769–10790

36. Iacovoni, J. S., Caron, P., Lassadi, I., Nicolas, E., Massip, L., Trouche, D., and Legube, G. (2010) High-resolution profiling of gammaH2AX around DNA double strand breaks in the mammalian genome. *EMBO J.* **29**, 1446–1457

37. Clouaire, T., Rocher, V., Lashgari, A., Arnould, C., Aguirrebengoa, M., Biernacka, A., Skrzypczak, M., Aymard, F., Fongang, B., Dojer, N., Iacovoni, J. S., Rowicka, M., Ginalski, K., Côté, J., and Legube, G. (2018) Comprehensive mapping of histone modifications at DNA double-strand breaks deciphers repair pathway chromatin signatures. *Mol. Cell* **72**, 250–262.e6

38. Li, M., Bian, C., and Yu, X. (2014) Poly(ADP-ribosyl)ation is recognized by ECT2 during mitosis. *Cell Cycle* **13**, 2944–2951

39. Huff, L. P., Decristo, M. J., Trembath, D., Kuan, P. F., Yim, M., Liu, J., Cook, D. R., Miller, C. R., Der, C. J., and Cox, A. D. (2013) The role of Ect2 nuclear RhoGEF activity in ovarian cancer cell transformation. *Genes Cancer* **4**, 460–475

40. Wang, H., Liu, H., Li, J., Wei, S., Liu, X., Wan, H., Zheng, P., and Zheng, H. (2020) Effect of Ect2 expression on the growth of triple-negative breast cancer cells with paclitaxel intervention. *Onco Targets Ther.* **13**, 12905–12918

41. Daulat, A. M., Finetti, P., Revinski, D., Silveira Wagner, M., Camoin, L., Audebert, S., Birnbaum, D., Kodjabachian, L., Borg, J. P., and Bertucci, F. (2019) ECT2 associated to PRICKLE1 are poor-prognosis markers in triple-negative breast cancer. *Br. J. Cancer* **120**, 931–940

42. Xiu, Y., Liu, W., Wang, T., Liu, Y., and Ha, M. (2019) Overexpression of ECT2 is a strong poor prognostic factor in ER(+) breast cancer. *Mol. Clin. Oncol.* **10**, 497–505

43. Wang, H. K., Liang, J. F., Zheng, H. X., and Xiao, H. (2018) Expression and prognostic significance of ECT2 in invasive breast cancer. *J. Clin. Pathol.* **71**, 442–445

44. Li, M., and Yu, X. (2013) Function of BRCA1 in the DNA damage response is mediated by ADP-ribosylation. *Cancer Cell* **23**, 693–704

45. Li, M., Lu, L. Y., Yang, C. Y., Wang, S., and Yu, X. (2013) The FHA and BRCT domains recognize ADP-ribosylation during DNA damage response. *Genes Dev.* **27**, 1752–1768

46. Sheng, Z. Z., Zhao, Y. Q., and Huang, J. F. (2011) Functional evolution of BRCT domains from binding DNA to protein. *Evol. Bioinform. Online* **7**, 87–97

47. Mordes, D. A., Glick, G. G., Zhao, R., and Cortez, D. (2008) TopBP1 activates ATR through ATRIP and a PIKK regulatory domain. *Genes Dev.* **22**, 1478–1489

48. Kumagai, A., Lee, J., Yoo, H. Y., and Dunphy, W. G. (2006) TopBP1 activates the ATR-ATRIP complex. *Cell* **124**, 943–955

49. Saito, S., Liu, X. F., Kamijo, K., Raziuddin, R., Tatsumoto, T., Okamoto, I., Chen, X., Lee, C. C., Lorenzi, M. V., Ohara, N., and Miki, T. (2004) Deregulation and mislocalization of the cytokinesis regulator ECT2 activate the Rho signaling pathways leading to malignant transformation. *J. Biol. Chem.* **279**, 7169–7179

50. Kim, J. E., Billadeau, D. D., and Chen, J. (2005) The tandem BRCT domains of Ect2 are required for both negative and positive regulation of Ect2 in cytokinesis. *J. Biol. Chem.* **280**, 5733–5739

51. Bement, W. M., Leda, M., Moe, A. M., Kita, A. M., Larson, M. E., Golding, A. E., Pfeuti, C., Su, K. C., Miller, A. L., Goryachev, A. B., and von Dassow, G. (2015) Activator-inhibitor coupling between Rho signalling and actin assembly makes the cell cortex an excitable medium. *Nat. Cell Biol.* **17**, 1471–1483

52. Justilien, V., Lewis, K. C., Meneses, K. M., Jamieson, L., Murray, N. R., and Fields, A. P. (2020) Protein kinase Cι promotes UBF1-ECT2 binding on ribosomal DNA to drive rRNA synthesis and transformed growth of non-small-cell lung cancer cells. *J. Biol. Chem.* **295**, 8214–8226

53. Tanaka, I., Chakraborty, A., Saulnier, O., Benoit-Pilven, C., Vacher, S., Labiod, D., Lam, E. W. F., Bièche, I., Delattre, O., Pouzoulet, F., Auboeuf, D., Vagner, S., and Dutertre, M. (2020) ZRANB2 and SYF2-mediated splicing programs converging on ECT2 are involved in breast cancer cell resistance to doxorubicin. *Nucleic Acids Res.* **48**, 2676–2693

54. O'Connor, M. J. (2015) Targeting the DNA damage response in cancer. *Mol. Cell* **60**, 547–560

55. Blackford, A. N., and Jackson, S. P. (2017) ATM, ATR, and DNA-PK: The trinity at the heart of the DNA damage response. *Mol. Cell* **66**, 801–817

56. Wang, Q., Ma, S., Song, N., Li, X., Liu, L., Yang, S., Ding, X., Shan, L., Zhou, X., Su, D., Wang, Y., Zhang, Q., Liu, X., Yu, N., Zhang, K., *et al.* (2016) Stabilization of histone demethylase PHF8 by USP7 promotes breast carcinogenesis. *J. Clin. Invest.* **126**, 2205–2220

57. Ma, J., Chen, T., Wu, S., Yang, C., Bai, M., Shu, K., Li, K., Zhang, G., Jin, Z., He, F., Hermjakob, H., and Zhu, Y. (2019) iProX: An integrated proteome resource. *Nucleic Acids Res.* **47**, D1211–D1217

ASBMB

J. Biol. Chem. (2021) 297(3) 101036 **15**